# Field-Reversed Configuration Maintained by Rotating Magnetic Field with High Spatial Harmonics

Michiaki Inomoto, Katsuhisa Kitano, and Shigefumi Okada

*Center for Atomic and Molecular Technologies, Graduate School of Engineering, Osaka University, Osaka 565-0871, Japan*

(Received 11 April 2007; published 26 October 2007)

Field-reversed configurations (FRCs) driven by rotating magnetic fields (RMFs) with spatial high harmonics have been studied in the metal flux conserver of the FRC injection experiment. The experimental results show that the fundamental RMF component is observed to penetrate the plasma column, while the high harmonics are screened at the plasma edge due to their slower or reversed rotation. This selective penetration of the RMF provides good compatibility of radial and azimuthal force balances; significant radial inward force $\langle \tilde{j}_z \tilde{B}_\theta \rangle$ mostly from the high-harmonic components, and sufficient azimuthal torque solely provided by the fundamental component.

DOI: 10.1103/PhysRevLett.99.175003 PACS numbers: 52.55.Lf, 52.55.Wq

A field-reversed configuration (FRC) is a compact toroid confined solely by poloidal magnetic field [1]. It has an extremely high-$\beta$ value close to unity, which is advantageous as a magnetic confinement system. As a promising current drive method of the FRC, transverse rotating magnetic field (RMF) [2] has been extensively studied experimentally [3–6] and numerically [7–9]. Following successful demonstration of the formation and quasisteady sustainment of FRC plasmas by some apparatus using symmetric dipole RMF, some novel RMF configurations have been recently proposed, such as asymmetric RMF [10–12] and quadrupole RMF [13] to improve plasma performance or current drive efficiency.

In this Letter, we demonstrate some novel features of the FRC sustained by the RMF inside a metal chamber. Since the RMF does not penetrate the conducting vessel wall, the RMF antennas must be located inside the vessel. The metal chamber wall yields two unique features on RMF current drive; first, the field lines of the RMF do not penetrate or cross the vessel wall. This will provide better energy and particle transport properties than the RMF generated by antennas located outside the vessel. The other is that the RMF has significant magnitude of spatial high-harmonic components due to the facts that the antennas are located closer to the plasma and the eddy current is induced on the wall. The difference in the rotation frequency between the fundamental and the spatial high-harmonic components provides selective penetration of the RMF to the plasma column. The fundamental RMF component which penetrates up to the center of the plasma column gives sufficient azimuthal torque to the plasma and the screened high-harmonic components exert a magnetic pressure to prevent the plasma to expand, limiting the plasma separatrix radius to $x_s = r_{\Delta\phi}/r_w < 0.65$, which is small compared with the FRCs observed in previous RMF experiments.

The impact of spatial high harmonics is evaluated by using a one-dimensional model of an FRC driven by the RMF. The alternating RMF is expressed by the vector potential $\boldsymbol{A}$ as

$$\nabla^2 \tilde{A}_z + \mu_0 \tilde{j}_z = 0. \quad (1)$$

Here, the variables with a tilde indicate that they are the alternating quantities originating from the RMF antenna current flowing in $z$ direction. The vacuum solution based on the assumption that the chamber wall ($r_w = 0.4$ m) is a perfect conductor is shown in Fig. 1(a) for three different phase timings, together with the antenna arrangement. It is obvious that the total RMF consists of magnetic fields with odd azimuthal mode numbers $m = 1, 3, 5, \ldots$, since the antennas are arranged to have $m = 1$ azimuthal symmetry. These spatial high-harmonic components become significant when the antennas are close to the object domain and are enhanced by the eddy current on the conducting wall outside the antennas. The radial profiles of vacuum $|A_z|$ and $|B_\theta|$ together with their azimuthal mode components of $m = 1$, 3, 5 are shown in Figs. 2(a) and 2(b). The

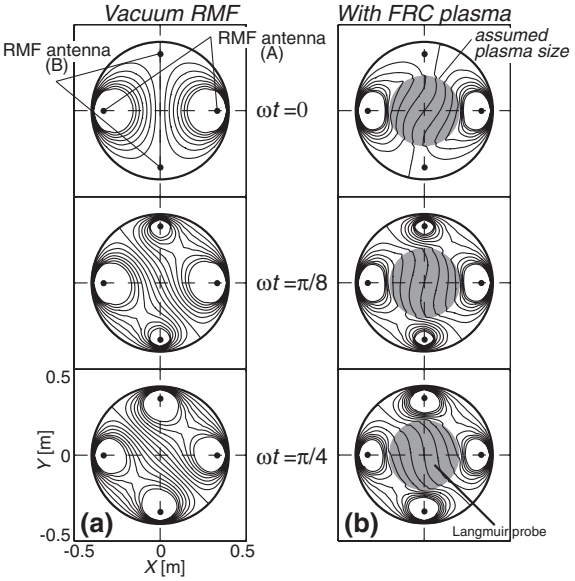


FIG. 1. Field structure of the RMF inside the conducting vessel (a) without and (b) with FRC plasma.

 

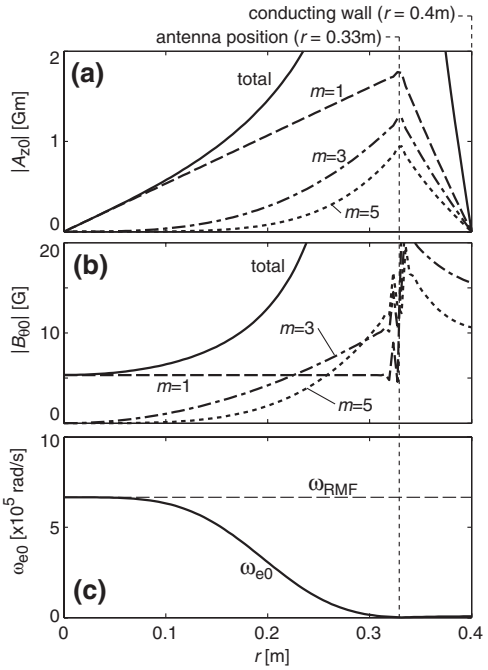


FIG. 2. Radial profiles of (a) the vector potential, (b) azimuthal magnetic field of the RMF, and (c) synchronous rotation frequency in vacuum.

fundamental $|B_\theta|$ is uniform inside the antenna position, and the high-harmonic components rise at outer radial position. Since two pairs of antennas are employed in this experiment, the currents alternating with angular frequency $\omega$ on each pair of antennas have phase difference of $\pi/2$, hence, the vector potential or other alternating variables resulting from the RMF will have the form of

$$\begin{aligned}\tilde{X} &= \sum_m X_m \cos m\theta \sin\omega t \\ &\quad + \sum_m X_m \cos m(\theta - \pi/2) \sin(\omega t - \pi/2), \\ &= X_1 e^{i(\omega t-\theta)} + X_3 e^{i(\omega t+3\theta)} + X_5 e^{i(\omega t-5\theta)} \\ &\quad + X_7 e^{i(\omega t+7\theta)} + \cdots,\end{aligned} \tag{2}$$

where $m = 1, 3, 5, \cdots$. The spatial high harmonics with mode $m = 2k - 1 (k = 1, 2, 3, \cdots)$ rotate with the angular frequency of $\pm\omega/m$, where the sign is positive for odd $k$ number (or $m = 1, 5, 9, \cdots$) and negative for even $k$ number (or $m = 3, 7, 11, \cdots$). Thus the high harmonics have slower or reversed rotation frequency compared with the fundamental component. This behavior is just the same as the multipolar induction motors and has some similarities to the frequency modulated RMF [14,15].

The axial component of the electron's equation of motion is expressed as

$$\tilde{E}_z = \eta_\parallel \tilde{j}_z + \omega_e r\tilde{B}_r + \frac{m_e}{e^2 n_e} i\omega \tilde{j}_z = \eta_\parallel^* \tilde{j}_z + \omega_e r\tilde{B}_r, \tag{3}$$

where $\eta_\parallel$ is the parallel classical resistivity, $\eta_\parallel^* = \eta_\parallel + i\omega \frac{m_e}{e^2 n_e}$ is the effective resistivity, and $\omega_e$ is the electron rotation angular frequency. Then the screening current flowing in the plasma is expressed as

$$\begin{aligned}\tilde{j}_z &= \frac{1}{\eta_\parallel^*}(\tilde{E}_z - \omega_e r\tilde{B}_r) = \frac{1}{\eta_\parallel^*}\left(-\frac{\partial}{\partial t} - \omega_e \frac{\partial}{\partial\theta}\right)\tilde{A}_z \\ &= -\frac{1}{\eta_\parallel^*}(i\omega + \omega_e \frac{\partial}{\partial\theta})\tilde{A}_z.\end{aligned} \tag{4}$$

Now the radial profiles of the time-independent part of $|A_z|$ and other alternating variables with their phase information can be calculated using Eqs. (1) and (4) for the given radial profile of $\omega_e$, which is determined from azimuthal force balance of the FRC.

The FRC equilibrium driven by the RMF should satisfy both radial and azimuthal force balance. The radial pressure balance equation is written as follows, assuming uniform ion and electron temperatures and the fixed ions,

$$j_\theta B_z - \langle \tilde{j}_z \tilde{B}_\theta \rangle = \frac{\partial p}{\partial r} \approx k(T_i + T_e)\frac{\partial n_e}{\partial r}, \tag{5}$$

where $j_\theta = -en_e\omega_e r$, $\tilde{B}_\theta = -\partial\tilde{A}_z/\partial r$, and the bracket $\langle\rangle$ represents average over an RMF cycle. The azimuthal force balance equation is expressed as

$$f_{\theta,\mathrm{coll}} = f_{\theta,\mathrm{RMF}}, \tag{6}$$

where

$$f_{\theta,\mathrm{coll}} = \nu m_e n_e \omega_e r, \tag{7}$$

$$\begin{aligned}f_{\theta,\mathrm{RMF}} &= \langle \tilde{j}_z \tilde{B}_r \rangle = \left\langle -\frac{1}{\eta_\parallel^*}\left(i\omega + \omega_e \frac{\partial}{\partial\theta}\right)\tilde{A}_z \frac{1}{r}\frac{\partial\tilde{A}_z}{\partial\theta}\right\rangle \\ &= \sum_m \frac{1}{2\eta_\parallel^*}(\omega \mp m\omega_e)\frac{\mp m}{r}A_{z,m}^2.\end{aligned} \tag{8}$$

Figure 2(c) shows the vacuum synchronous rotation frequency $\omega_{e0}$ derived from $f_{\theta,\mathrm{RMF}} = 0$, which indicates the local averaged rotation frequency in vacuum. The synchronous frequency is decelerated at the outer region where the spatial high harmonics with slower or reversed rotation becomes significant and no rotation is expected in the vicinity of the antenna. Because of the large radial variation of the synchronous frequency, the azimuthal force balance equation must be satisfied locally. Hence, the FRC equilibrium with quite large separatrix radius, which has been often observed in previous RMF experiments [3–6,13], might not be feasible in this system.

Figure 3 shows the schematic of the confinement section of the FRC injection experiment (FIX), where two pairs of RMF antennas are installed at $r = 0.33$ m inside the conducting vessel wall made of 6 mm thick stainless steel. The antennas have length of 1.2 m and are covered by ceramic tubes. Preionized deuterium gas is supplied by a washer gun located on the midplane of the device. Two radial magnetic probe arrays are used to measure both steady

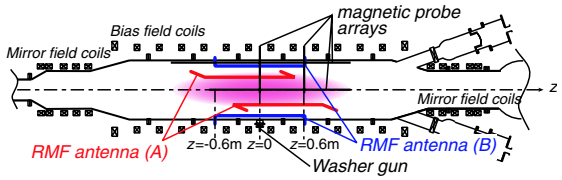


FIG. 3 (color online). Side view of the confinement chamber of the FIX apparatus.

$B_z$ and alternating $\tilde{B}_\theta$. Electron density is measured by a Langmuir probe.

Figure 4 shows time evolutions of (a) RMF antenna currents, (b) steady axial magnetic field measured at $r = 0.25$ m (outside the plasma) and $r = 0$ (inside the plasma), and (c) separatrix and major radii. The RMF current with angular frequency of $\omega = 670 \times 10^3$ rad/s is applied for more than 1 ms. The washer gun discharge starts at about $t = 0.3$ ms and highly ionized plasma is injected into the central region of the device, where the RMF is already applied. After the initial unstable period, the RMF begins to drive current, forming an FRC after $t = 0.6$ ms. The magnetic field inside the plasma shows large reversal (strength of the reversed field at the center is larger than that of the external field) without serious instability during the RMF discharge period of about 0.8 ms, which corresponds to ~50 Alfvén transit time. The global stability might be provided by the kinetic effect since the ion collisionless skin depth is even larger than the separatrix radius. Plasma shape is almost unchanged and the separatrix radius is about $r_{\Delta\phi} = 0.25$ m, yielding $x_s = r_{\Delta\phi}/r_w \sim 0.625$. This value is much smaller than those observed in previous results from purely dipole RMF [3–6] and recent quadrupole RMF experiments [13]. The separatrix length is $l_s = 0.8$–$1.0$ m, keeping moderate elongation of about 2. Typical plasma parameters are as follows; ion and electron cyclotron frequencies $\omega_{ci} = 34 \times 10^3$ rad/s and $\omega_{ce} = 120 \times 10^6$ rad/s, electron-ion collision frequency $\nu_{ei} = 1.1 \times 10^6$ rad/s, peak plasma density $n_m = 7 \times 10^{17}$ m$^{-3}$, and electron temperature $T_e \leq 10$ eV.

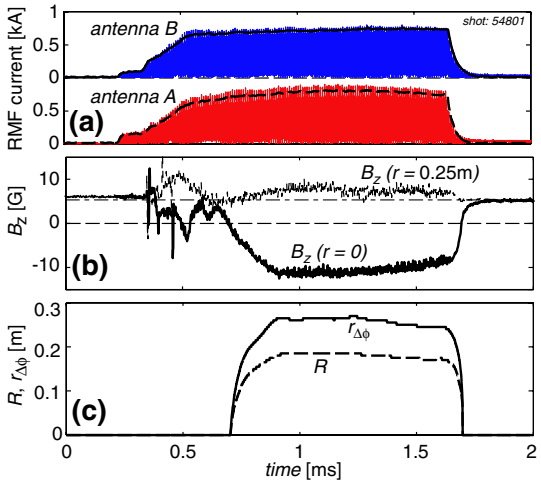


FIG. 4 (color online). Time evolutions of (a) RMF antenna currents, (b) axial magnetic field, and (c) separatrix and major radii.

Radial profiles of various physical quantities observed during $t = 1.0$–$1.2$ ms are shown in Fig. 5, together with the numerical results. Here, the numerical solution which satisfies the Eqs. (1) and (4)–(6) simultaneously at every radial position is obtained by iterative method with several given parameters, such as RMF antenna current, RMF frequency, initial bias field, electron temperature, and the total electron inventory per unit length. Note that the non-alternating variables, such as $n_e$ and $\omega_e$, are assumed to be axisymmetric in this calculation. The two-dimensional field structure obtained from the calculation is shown in Fig. 1(b). It is observed that only the $m = 1$ component of the RMF penetrates into the plasma, keeping almost constant spatial structure in the plasma region, while the RMF outside the plasma region has large spatial high-harmonic components, the structure of which changes with time.

Figure 5(a) shows the radial profile of the RMF $|B_\theta|$ measured by the magnetic probe array (circle symbols) together with the numerical result (solid line). The experimental result shows that large part of the RMF is screened at the plasma edge ($r \sim 0.17$ m), although certain magnitude of the RMF reaches the center. The numerical result shows similar behavior; the $m = 1$ component penetrates up to the plasma center while the high harmonics such as $m = 3, 5, \cdots$ are absolutely screened and generate large gradient at the plasma surface. The gradient in numerical result locates, however, somewhat outboard side compared with the experimental result. Nevertheless, on the whole, the numerical results generally agree well with the experimental results. The dimensionless parameters of $\gamma = \omega_{ce}/\nu_{ei}$ and $\lambda = r_s/\sqrt{2\eta_\parallel/\mu_0\omega}$ are often used to evaluate the penetration condition of the RMF [7,8]. In this experiment, these quantities have the values of $\gamma \sim 120$ and $\lambda \sim 30$–$40$, which satisfy the full penetration condition of $\gamma > 1.12\lambda$ [8] for the fundamental component of the RMF. Figure 5(b) shows the radial profile of the electron rotation angular frequency obtained from the numerical model. The synchronous rotation region is seen to expand compared with the vacuum case. The reason is that the high-harmonic components are screened by the plasma on one hand, but the fundamental component is not on the other. The entire plasma column rotates with frequency close to $\omega$, since only the fundamental component penetrates the plasma. Note that there is slow rotation region at $r > 0.2$ m, where the fundamental component is also thought to be screened, but the numerical result shows no plasma density at that region, as shown in Fig. 5(c). Therefore, the equilibrium can be expressed in such a way that the plasma must be confined just inside the synchronous rotation region, otherwise even a fundamental component of the RMF will not penetrate the plasma and the FRC equilibrium will never be sustained. Whereas the experimental result shows that a

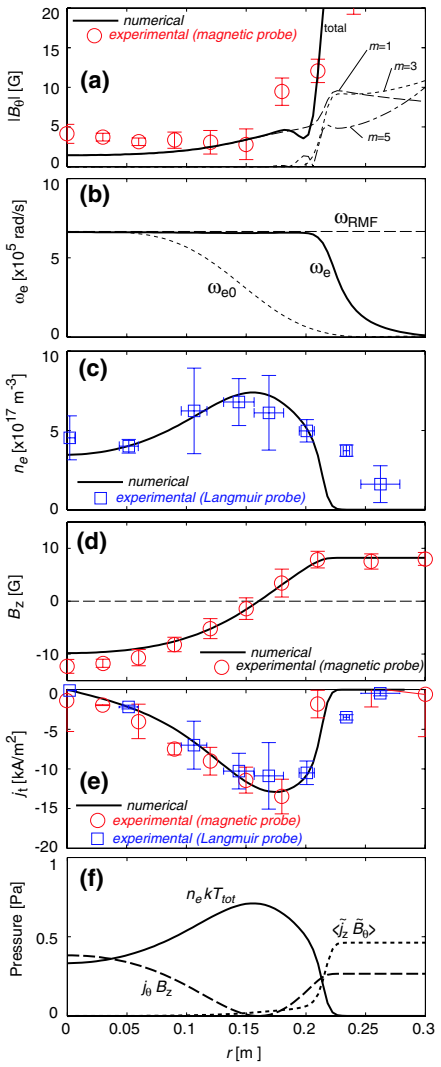


FIG. 5 (color online). Radial profiles of (a) amplitude of RMF, (b) electron rotation angular frequency, (c) electron density, (d) axial magnetic field, (e) toroidal current density, and (f) thermal and magnetic pressures.

certain amount of plasma exists outside the separatrix, possibly because the Langmuir probe measurement was carried out at the toroidal position in between two antennas [see bottom panel of Fig. 1(b)], where the magnetic pressure of the RMF may not be large enough to get rid of the plasma.

Figure 5(d) shows the radial profile of the steady axial magnetic field $B_z$. The experimental and the numerical profiles show good agreement in shape and amplitude, except for the region near the center. Both experimental and numerical profiles of $B_z$ become flat at the outer region ($r > 0.2$ m), indicating no current flowing in that region. Figure 5(e) shows the radial profile of the toroidal current density $j_t$. The solid line represents the numerical result, the circle symbols are radial derivatives of experimentally measured $B_z$, and the square symbols are calculated from $j_\theta = -en_e\omega_e r$ using experimentally measured $n_e(r)$ and numerical $\omega_e(r)$. These profiles agree well and show small current density at $r > 0.2$ m, as expected from the calculation. Figure 5(f) shows the radial profiles of thermal and magnetic pressures obtained from the model. The plasma pressure is sustained by both the steady $j_\theta B_z$ force in usual FRC equilibrium and the time average of $\tilde{j}_z\tilde{B}_\theta$. Since the $m = 1$ fundamental component almost fully penetrates the plasma column, the spatial high-harmonic components mainly contribute the $\langle\tilde{j}_z\tilde{B}_\theta\rangle$ force, which becomes even larger than the $j_\theta B_z$ force.

In summary, a novel FRC equilibrium driven by the RMF with high harmonics has been investigated experimentally and discussed using 1D numerical model. The fact that the high harmonics rotate with frequency $\pm\omega/m$ yields that the synchronously rotating plasma column will screen the high-harmonic components near the plasma edge. This unique feature of the selective penetration has effects on both azimuthal and radial force balance. The azimuthal driving force mainly comes from the fundamental $m = 1$ component of the RMF while the high harmonics contribute to generate large inward force at the plasma edge, keeping the separatrix radius far from the chamber wall.

The authors would like to thank the FIX group members for their technical support and Professor Y. Ono for provision of washer gun technique. This work was partly supported by the Grant-in-Aid for Scientific Research No. 14380212 of the Japan MEXT.

[1] M. Tuszewski, Nucl. Fusion **28**, 2033 (1988).
[2] H. A. Blevin and P. C. Thonemann, Nucl. Fusion, part 1, **55** (1962).
[3] I. R. Jones, Phys. Plasmas **6**, 1950 (1999).
[4] J. T. Slough and K. E. Miller, Phys. Plasmas **7**, 1945 (2000).
[5] H. Y. Guo *et al.*, Phys. Plasmas **9**, 185 (2002).
[6] A. L. Hoffman, H. Y. Guo, K. E. Miller, and R. D. Milroy, Nucl. Fusion **45**, 176 (2005).
[7] W. N. Hugrass, Aust. J. Phys. **38**, 157 (1985); **39**, 513 (1986).
[8] R. D. Milroy, Phys. Plasmas **6**, 2771 (1999); **7**, 4135 (2000).
[9] M. Ohnishi and A. Ishida, Phys. Plasmas **9**, 2633 (2002).
[10] S. A. Cohen and R. D. Milroy, Phys. Plasmas **7**, 2539 (2000).
[11] H. Y. Guo, A. L. Hoffman, and L. C. Steinhauer, Phys. Plasmas **12**, 062507 (2005).
[12] S. A. Cohen *et al.*, Phys. Rev. Lett. **98**, 145002 (2007).
[13] R. D. Milroy and H. Y. Guo, Phys. Plasmas **12**, 072503 (2005).
[14] R. A. Clemente, J. Phys. Soc. Jpn. **67**, 3450 (1998).
[15] W. N. Hugrass, Plasma Phys. Controlled Fusion **42**, 1219 (2000).